On-Line Identification via Haar Wavelet Expansions

Jin-Wei Liang

Department of Mechanical Engineering, Ming Chi University of Technology, New Taipei City, 24306, TAIWAN

liangj@mail.mcut.edu.tw

***Abstract*- This paper develops an on-line identification algorithm to estimate system parameters of non-linear continuous time systems. The algorithm, based on Haar wavelet expansions, uses the observed input-output data to estimate unknown system parameters. A recursive formula augmented with indirect matrix-inversion schemes is proposed to substantially reduce computation requisites of an existed off-line scheme. By means of the proposed algorithm, the parameter estimates are real-time updated without repeatedly computing matrix inversions. The latter is most time-consuming in accomplishing every chronological identification operation. The convergences of the off-line and on-line algorithms under noise-free condition are shown. The algorithm is validated through numerical and experimental examples in which the reliability and effectiveness of the proposed approach have been demonstrated.**

Keywords- On-line Identification; Haar Wavelet Expansion; Recursive Formula

I. INTRODUCTION

System identification techniques can be roughly divided into nonparametric and parametric, depending on the preliminary knowledge of the target system [1, 2]. In parametric identification, the preliminary knowledge of the system is sufficient to write down a specific form of differential equation of motion with some unknown coefficients. These coefficients can be identified using input and output signals of the system. The non-parametric methods have intrinsic problems related to the mathematical complexity, convergence rate, and excessive computational time that make them not suitable for on-line identifications.

Modelling and identification of non-linear dynamic system is a challenging task because non-linear processes are unique in the sense that they do not share many properties. The principle of superposition is not valid for non-linear systems. Thus, most linear analysis techniques are not applicable. In recent years, a number of alternative approaches have been proposed for the identification of non-linear dynamical structural systems. For instance, the ARMA models used for linear system identification are extended to deal with non-linear systems through the NARMAX models [3]. The main idea is to non-linearly regress the current response data point on the past response and input data points. The limitations of the procedures are their significant computation requisites, and the lack of physical significance to be attributed to many of the associated parameters. In contrast, a direct parameter estimation method has been proposed in [4] where both linear and non-linear elements are postulated at certain locations throughout a discrete model of the system. The model parameters are then estimated by curve fitting the data with the assumed model through least-squares techniques. The most appropriate set of parameters to include in the model is obtained through a statistical significance test. The method is also limited by its significant computation requisites.

There are other methods that can be used for non-linear parametric identification. These include those of Gottlieb *et al.* [5] and Feldman [6], which employed the Hilbert transform. Many orthogonal functions have also been introduced to project nonlinear differential equation of motion onto different basis function so as to identify unknown system parameters [7-13]. When using the method of orthogonal function expansions, the dynamic equations of the system are transformed into a set of algebraic equations with the system parameters as unknowns. These algebraic equations can then be solved in the least-squares sense.

Unlike the above-mentioned methods, the wavelet-based procedure for the identification of non-linear systems has dual localization properties in time and frequency domains. The frequency localization property of wavelets can be used to decouple closely spaced modes of vibration. On the other hand, the time-domain localization permits the tracking of fast variations of the states of the dynamical system that would have been averaged out using other techniques. Many research attempts thus apply the wavelet transform for the identification of the non-linear system. For instance, [14] takes advantage of the time-scale properties of the wavelet functions to analyze non-linear vibrations. The wavelet-transform ridges and skeletons of the system impulse response were adopted to extract the frequency characteristics and decay envelope. The continuous Morlet-wavelet transform provides the necessary mode decoupling thanks to the frequency localization of the wavelets. Differently, in [15] the wavelet time localization property was utilized where Daubechies scaling functions were used to express the tangent stiffness. The hysteresis curves and damping coefficients were identified. It is conceivable that the dual localization properties of wavelet transform could be very advantageous to parameter-identification tasks so long as proper basis were chosen based on the characteristics of system states and input signal.

Recently, the Haar-wavelet-based approach has attracted much attention due to its simple but analytical expression [16-20]. Haar wavelet is an orthogonal set. Therefore, it shares those nice properties possessed separately by orthogonal series expansion and wavelet transform. Moreover, Haar basis contains only a finite number of non-zero values in a bounded time interval. This property substantially reduces the computation efforts required in obtaining the orthogonal expansion coefficients. Since these expansion coefficients are needed in identifying

unknown system parameters which makes Haar wavelet an excellent candidate for implementing the on-line identification tasks.

II. THE HAAR-WAVELET-BASED IDENTIFICATION ALGORITHM

A. Haar Wavelet Expansions

The orthogonal Haar basis $\{h_n(t),\ n \in Z^+\}$ can be used to represent any function $f(t)$ in $L^2[0,1)$ [21], so that

$$f(t) = \sum_{n=0}^{\infty} c_n h_n(t) \tag{1}$$

where

$$h(t) = \begin{cases} 1, & 0 \le t < 1/2 \\ -1, & 1/2 \le t < 1 \\ 0, & otherwise \end{cases}$$

and

$$h_0(t) = 1$$
$$h_1(t) = h(t)$$
$$h_n(t) = h(2^j t - k),\ \ n = 2^j + k,\ \ j \ge 0,\ \ 0 \le k < 2^j$$

In addition, the orthogonal property of the Haar basis leads to the following relationship

$$\int_0^1 h_i(t) h_l(t) dt = 2^{-j} \delta_{il} = \begin{cases} 2^{-j}, i = l = 2^j + k, & j \ge 0,\ \ 0 \le k < 2^j \\ 0, & i \ne l \end{cases} \tag{2}$$

According to Eq. (2), the expansion coefficients c_n in Eq. (1) can be determined by using the following inner product

$$c_n = 2^j \int_0^1 f(t) h_n(t) dt$$

where "*j*" is a non-negative integer. Its definition is the same as that in Eq. (2). Representing a signal with an infinite set of basis functions in most of time is not practical. To that end, the signal can be approximated using a truncated Haar basis functions as the following

$$f(t) \approx \sum_{n=0}^{m-1} c_n h_n(t) = c_{(m)}^T h_{(m)}(t) \tag{3}$$

where $m = 2^i$, $i \ge 0$, and

$$c_{(m)} = [c_0 \quad c_1 \cdots c_{m-1}]^T$$

$$h_{(m)}(t) = [h_0(t) \quad h_1(t) \cdots h_{m-1}(t)]^T \tag{4}$$

where "*T*" indicates transposition, and the subscript *m* in the parentheses denotes the number of Haar basis. In digital implementations, the following row vector can be adopted to represent the sampled data of $h_n(t)$ [21]

$$v_n = \left[h_n\left(\frac{1}{2m}\right) \quad h_n\left(\frac{3}{2m}\right) \cdots h_n\left(\frac{2m-1}{2m}\right) \right]$$

for $0 \le n < m$. Then, there is one-to-one correspondence between the row vector v_n and the Haar wavelet $h_n(t)$. Take $m = 2^2 = 4$ as an example, we have

$$h_0(t) \Leftrightarrow v_0 = [1 \ \ 1 \ \ 1 \ \ 1]$$
$$h_1(t) \Leftrightarrow v_1 = [1 \ \ 1 \ \ -1 \ \ -1]$$
$$h_2(t) \Leftrightarrow v_2 = [1 \ \ -1 \ \ 0 \ \ 0]$$
$$h_3(t) \Leftrightarrow v_3 = [0 \ \ 0 \ \ 1 \ \ -1]$$

v_n can be interpreted as the digital representation of $h_n(t)$. One usually replaces $h_n(t)$ with v_n to speed up the associated computations. As a consequence, suppose that *m* Haar basis functions $h_{(m)}(t) \in R^m$ are used for expansion. The following representation can be applied

$$H_{(m)} = [v_0 \quad v_1 \cdots v_{m-1}]^T \tag{5}$$

Here, $H_{(m)}$ is the digital representation of $h_{(m)}(t)$, and will be denoted as the "operational matrix of expansion," hereafter.

B. The Off-Line Identification Algorithm

The off-line identification scheme based on "finite" Haar series expansion is briefed in this section. In Chen [21], a system resembling to the following nonlinear time-invariant model represented in the state-space form is considered

$$\dot{x}(t) = f(x) + D(x)\theta + Bu(t) \tag{6}$$

where $x \in R^n$ is the state vector, $f: R^n \to R^n$ and $D: R^n \to R^{n \times p}$ are known functions of the states. $\theta \in R^p$ contains the "un-identified" parameters. $B \in R^{n \times s}$ is assumed to be known while $u \in R^s$ represents the input. In addition, $D(x) = [d_{ij}(x)]$. $D(x)$ is assumed to be of full rank for each x in Ω where Ω is the domain of interest. θ is the unknown "constant" parameter vector. It is worth to note that the Harr-based expansion method is not limited to constant-parameter identification. For instance, in [22], Chen studied a time-varying system where the un-identified parameters are functions of time. Unlike [21] in which an input-free case was studied, here we investigate a forced system. Meanwhile, all the state functions of the nonlinear time-invariant system presented in (6) are assumed to be known while the associated parameters are to be identified.

Suppose that all of the time functions appearing in equation (6) are "approximated" by the truncated Haar basis functions, $h_{(m)}(t)$, and only one initial condition, $x(t_0) = x_0$, is considered. Then, the following relationships hold

$$x(t) \approx F h_{(m)}(t) \tag{7}$$

$$\dot{x}(t) \approx F_d h_{(m)}(t) \tag{8}$$

$$f(x(t)) \approx F_f h_{(m)}(t) \tag{9}$$

$$d_{ij}(x(t)) \approx f_{ij}^T h_{(m)}(t) \tag{10}$$

$$u(t) \approx G h_{(m)}(t) \tag{11}$$

where $F \in R^{n\times m}$, $F_d \in R^{n\times m}$, $F_f \in R^{n\times m}$, $f_{ij} \in R^m$, and $G \in R^{s\times m}$. Additionally, the following relationship has been derived in [21]

$$D(x(t))\theta \approx \hat{D}(\theta \otimes I_m)h_{(m)}(t) \tag{12}$$

where $\otimes$ denotes the Kronecker product and $\hat{D}$ is an $n \times mp$ matrix composed of $n \times p$ blocks of dimension $1\times m$. The *ij*-th block of $\hat{D}$ is f_{ij}^T . Substituting Eqs. (8)-(12) into Eq. (6), yields

$$F_d h_{(m)}(t) = F_f h_{(m)}(t) + \hat{D}(\tilde{\theta} \otimes I_m)h_{(m)}(t) + BGh_{(m)}(t) \tag{13}$$

Here, " $\tilde{\theta}$ " is adopted to represent the "estimate" of unknown constant parameter vector because all the states and their related functions are approximated using finite Haar series. After some manipulation, the above equation can be recast into

$$\mathbf{vec}(F_d^T - F_f^T - (BG)^T) = \mathbf{vec}((\tilde{\theta} \otimes I_m)^T \hat{D}^T) \tag{14}$$

where the operator " **vec**(.) " transforms a matrix into a vector by appending its columns. Eq. (14) can be further organized as

$$\Gamma\tilde{\theta} = \alpha \tag{15}$$

in which $\alpha = \mathbf{vec}\,(F_d^T - F_f^T - (BG)^T)$, and Γ represents an $nm \times p$ matrix composed of $n \times p$ blocks of dimension $m \times 1$, so that the *ij*-th block of Γ is f_{ij} . If Γ is of full rank, the estimate of the unknown parameter, $\tilde{\theta}$, can be solved in the least-square sense, yielding

$$\tilde{\theta} = (\Gamma^T\Gamma)^{-1}\Gamma^T\alpha \tag{16}$$

Convergent identifications can be accomplished if Γ is of full rank. To ensure the full rank of Γ , the initial conditions and input signals should be rich enough so that the resultant state responses can fully demonstrate the system's characteristics or span the entire state space. Separate and specific conditions for gaining a full rank Γ were discussed in [21].

The implementation of the off-line process begins with the calculation of the Haar coefficient matrix F . From Eq. (7), F can be determined using $F = XH_{(m)}^{-1}$. Here $X \in \Re^{n\times m}$ is the digital representation of the measured state vector x . In contrast, F_d can be computed using the integration property of Haar basis and the knowledge of F . In other words, $F_d = (F - [x_0 \quad 0 \cdots 0])P_{(m)}^{-1}$, where $P_{(m)}$ is the "operational matrix of integration." $P_{(m)}$ can be obtained iteratively from the following equations [19]

$$P_{(m)} = \frac{1}{2m}\begin{bmatrix} 2mP_{(\frac{m}{2})} & -H_{(\frac{m}{2})} \\ H^{-1}_{(\frac{m}{2})} & 0 \end{bmatrix} \tag{17}$$

$$P_{(1)} = \frac{1}{2}$$

Next, F_f , f_{ij} , and G , can be calculated according to Eqs. (9)-(11). Based on these results, Γ and α can be formed, and then $\tilde{\theta}$ is calculated.

The content introduced so far are developed in [21] and denoted as the off-line identification algorithms. A couple of issues regarding the off-line scheme are of our concerns. Firstly, although Haar basis functions are defined for $t \in [0,1)$, in the real situations, the state responses and input function might exist for $0 \le t \le t_f$, or $t_0 \le t \le t_f$. Thus, a time-scale regulation is necessary. The regulation can be done by normalizing the real time variable or by modifying the values of $H_{(m)}$ and $P_{(m)}$, according to the length of the real time interval. The latter is adopted in this study. It turns out that only the value of $P_{(m)}$ changes when the real time interval is facing. The value of the other key operational matrix, $H_{(m)}$, remains the same.

To that end, the following expression for $P_{(m)}$ is derived as a substitute for Eq. (17) when a practical time interval is encountered

$$P_{(m)} = \frac{t_f^*}{2m}\begin{bmatrix} 2mP_{(\frac{m}{2})} & -H_{(\frac{m}{2})} \\ H^{-1}_{(\frac{m}{2})} & 0 \end{bmatrix} \tag{17a}$$

where $t_f^* = t_f - 0$, or $t_f - t_a$ depending on the initial time state.

Secondly, the calculations of F and F_d involve many matrix inversion operations, namely $H_{(m)}^{-1}$ and $P_{(m)}^{-1}$. These calculations are very time-consuming when the number of basis, m , is large. For instance, when $m = 512$, it takes about five seconds for a PC to compute $H_{(m)}^{-1}$ using the commercial software such as MATLAB. This is unacceptable since the real-time updating is quite impossible under such a slow speed, especially when more than one matrix inversion is involved in the scheme. To make the on-line identification task feasible, the cumbersome direct matrix inversion must be removed. Hence, simplified or indirect matrix-inversion algorithms are proposed in the next section.

III. THE ON-LINE IDENTIFICATION SCHEMES

On-line parameter identification has several advantages over the off-line counterpart. The primary one is that it can be used to progressively generate more accurate models, based on which the associated controllers can be continuously refined to improve the performance of the controlled system. Among the existing system-identification works employed orthogonal function expansions, very few are suitable for "on-line" identification. To the author's knowledge, the previous attempts can be found in the works done by Wu and Juang [23] and that by Chou *et al.* [24]. This study extends the existing off-line Haar-based scheme developed in [21] to handle the "on-line" adaptation task.

To accomplish the task, the computing time and computer memory of the original off-line schemes are to be reduced as much as possible. The proposed on-line, Haar-based identification algorithm consists of the indirect matrix inversions of $H_{(m)}$ and $P_{(m)}$ and the recursive identification formula. The derivations of these algorithms are covered below.

A. The Indirect Matrix Inversions of $H_{(m)}$ and $P_{(m)}$

Since the direct matrix inversion takes a lot of time when the number of basis is large, it has to be averted in the on-line scheme. Fortunately, by making use of some special features associated with $H_{(m)}$ and $P_{(m)}$ one can actually obtain $H_{(m)}^{-1}$ and $P_{(m)}^{-1}$ without involving direct inversions. To explain, let us first revisit the definition of $H_{(m)}$, namely

$$H_{(m)} = \begin{bmatrix} v_0 & v_1 \cdots v_{m-1} \end{bmatrix}^T \tag{5}$$

Next, we assume that the inverse of $H_{(m)}$ can be expressed as the following

$$H_{(m)}^{-1} = \begin{bmatrix} a_0 & a_1 \cdots a_{m-1} \end{bmatrix} \tag{18}$$

where $a_i \in \Re^m$, $i = 0 \cdots, m-1$ are column vectors with values undetermined. According to the matrix-inversion definition, the following relationship holds

$$H_{(m)} H_{(m)}^{-1} = \mathrm{I}_{(m)} \tag{19}$$

Moreover, the orthogonal property presented in Eq. (2) has the following digital representations

$$v_i v_l^T = \begin{cases} 2^{-j} m, & i = l = 2^j + k, \quad j \geq 0, \quad 0 \leq k < 2^j \\ 0, & i \neq l \end{cases} \tag{20}$$

where m is the dimension of the row vector v. Based on Eqs. (5) and (18)-(20), one can find out that the column vectors, a_i, $i = 0, \ldots m-1$, of Eq. (18) has the following simple form

$$a_i = \frac{2^j}{m} v_i^T, \quad i = 2^j + k, \quad j \geq 0, \quad 0 \leq k < 2^j \tag{21}$$

Thus, Eqs. (18) and (21) can be used to obtain $H_{(m)}^{-1}$. This approach is denoted as the indirect matrix inversion of $H_{(m)}$. In contrast with the direct-inversion approach which takes about five seconds to compute $H_{(512)}^{-1}$, the indirect inversion approach needs only less than one second to accomplish the same job.

We proceed to deal with the indirect inversion of $P_{(m)}$. According to Eq. (17a), one can obtain the following indirect matrix inversion of $P_{(m)}$ without much difficulty

$$P_{(m)}^{-1} = \frac{2m}{t_f^*} \begin{bmatrix} 0 & H_{(\frac{m}{2})} \\ -H_{(\frac{m}{2})}^{-1} & (2m) H_{(\frac{m}{2})}^{-1} P_{(\frac{m}{2})} H_{(\frac{m}{2})} \end{bmatrix} \tag{22}$$

where $t_f^* = t_f - 0$, or $t_f - t_a$ depending on the initial time state. Using Eq. (22) one can iteratively compute $P_{(m)}^{-1}$ from the knowledge of $H_{(m/2)}$, $H_{(m/2)}^{-1}$ and $P_{(m/2)}$, where $H_{(m/2)}^{-1}$ can be determined using the indirect approach presented in (21). Eqs. (18), (21), and (22) are denoted as the indirect matrix-inversion schemes of $H_{(m)}$ and $P_{(m)}$, respectively. These schemes, when incorporated with a recursive identification formula which will be derived in the next section, form the crux of the "on-line" identification algorithm.

B. The Recursive Identification Formula

In order to real-time update the system information the input-output data should be continuously fed to the identification process. The algorithm is denoted as a "moving" scheme in the literature, because the data-processing window is continuously marching forward to cover the most recent data. By moving the data window, iteration process is commonly employed to derive recursive formula. The recursive formula, computing the new parameters based on the knowledge obtained at the previous step and the incoming information, has a constant computation demand. Thus, it is suitable for on-line identification.

When windowing the data, a data-replacing action takes place at each updating step. In other words, during the replacing, the incoming data will replace all or part of the old data. The ratio of the length of the new-data vector to that of the old-data vector is denoted as the "data-replacing" ratio. In order to show how the iteration process works, let us suppose that the data-replacing ratio has been determined. Also, the following matrix representation is defined

$$\Gamma = \begin{bmatrix} \Gamma_a & \Gamma_b \end{bmatrix}^T \tag{23}$$

where Γ_a represents the sub-matrix corresponding to the "old" data, whereas Γ_b indicates the "new" data counterpart. If Eq. (23) is applied, Eq. (16) can be recast into the followings

$$\tilde{\theta}_{updated} = \left(\begin{bmatrix} \Gamma_a^T & \Gamma_b^T \end{bmatrix} \begin{bmatrix} \Gamma_a \\ \Gamma_b \end{bmatrix} \right)^{-1} \begin{bmatrix} \Gamma_a^T & \Gamma_b^T \end{bmatrix} \begin{bmatrix} \alpha_a \\ \alpha_b \end{bmatrix}$$

or

$$\tilde{\theta}_{updated} = \left[\Gamma_a^T \Gamma_a + \Gamma_b^T \Gamma_b \right]^{-1} \left[\Gamma_a^T \alpha_a + \Gamma_b^T \alpha_b \right]$$

Multiplying both sides of the above equation with $\left[\Gamma_a^T \Gamma_a + \Gamma_b^T \Gamma_b \right]$ leads to

$$\left[\mathrm{I} + (\Gamma_a^T \Gamma_a)^{-1} (\Gamma_b^T \Gamma_b) \right] \tilde{\theta}_{updated} = \tilde{\theta}_{old} + (\Gamma_a^T \Gamma_a)^{-1} \Gamma_b^T \alpha_b \tag{24}$$

in which $\tilde{\theta}_{old} = (\Gamma_a^T \Gamma_a)^{-1} \Gamma_a^T \alpha_a$. Eq. (24) can be further arranged into

$$\tilde{\theta}_{updated} = \left[\mathrm{I} + G_1 \right]^{-1} \left[\tilde{\theta}_{old} + \tilde{\theta}_{new} \right] \tag{25}$$

where $G_1 = (\Gamma_a^T \Gamma_a)^{-1} (\Gamma_b^T \Gamma_b)$ and $\tilde{\theta}_{new} = (\Gamma_a^T \Gamma_a)^{-1} \Gamma_b^T \alpha_b$. As expected, Eq. (25) indicates that the complete updated estimate indeed comprises of two parts: the information obtained from the previous step, $\left[\mathrm{I} + G_1 \right]^{-1} \tilde{\theta}_{old}$, and the correction made at the current step, $\left[\mathrm{I} + G_1 \right]^{-1} \tilde{\theta}_{new}$. Eq. (25)

is the so-called recursive formula, which can be applied to replace Eq. (16). The computation demand in implementing Eq. (25) is much less than that of Eq. (16). Hence, Eq. (25) when working with the indirect matrix inversion schemes can handle the on-line identification problems well. In the next section, the convergence of the infinite Haar-based identification algorithms under noise-free condition is shown.

IV. THE CONVERGENCE OF THE HAAR IDENTIFICATION ALGORITHMS

The identification schemes proposed here base on the orthogonal expansion theory. To that end, states, state functions, and input signal involved in the state equations are projected into different Haar basis. By doing that the state equations of the system are transformed into a set of algebraic equations with system parameters being the unknowns. These algebraic equations can then be solved using the least-squares criterion. In general, the number of the unknown system parameters is small while the number of Haar basis involved in the expansion can be increased without limits. Therefore, there always will be more equations than those required for solving the unknown parameters provided the states and input signal carry enough information.

In order to show the convergence of the Haar-based identification algorithms, we first denote the $L^2[0,1)$ space spanned by the orthogonal Haar basis, $\{h_n(t)\}$, as V. In addition, the subspace spanned by the finite Haar basis $h_{(m)}(t) \in R^m$ is denoted as V_1 while its complementary subspace, which is spanned by the "remainder" of the finite Haar series is denoted as V_2. Then, the following expression holds

$$V = V_1 \oplus V_2$$

Next, upon revisiting Eqs. (7)-(12) one can recast the followings

$$x(t) = Fh_{(m)}(t) + r_x(t)$$
$$\dot{x}(t) = F_d h_{(m)}(t) + r_{\dot{x}}(t)$$
$$f(x(t)) = F_f h_{(m)}(t) + r_f(t)$$
$$d_{ij}(x(t)) = f_{ij}^T h_{(m)}(t) + r_{d_{ij}}(t)$$
$$u(t) = Gh_{(m)}(t) + r_u(t)$$
$$D(x(t))\theta = \hat{D}(\theta \otimes I_{(m)})h_{(m)}(t) + r_D(t)$$

Here, $r_x(t)$, $r_{\dot{x}}(t)$, $r_f(t)$, $r_{d_{ij}}(t)$, $r_u(t)$, and $r_D(t)$ stand for the m-term finite Haar series "remainders" with respect to $x(t)$, $\dot{x}(t)$, $f(x(t))$, $d_{ij}(x(t))$, $u(t)$, and $D(x(t))\theta$, respectively. When the above expressions are substituted into Eq. (6), the following can be obtained

$$F_d h_{(m)}(t) + r_d(t) = F_f h_{(m)}(t) + r_f(t) + \hat{D}(\theta \otimes I_m)h_{(m)}(t) + r_D(t) + BGh_{(m)}(t) + r_u(t) \quad (26)$$

Here θ designates the parameter vector with "true" values obtaining using infinite Haar series expansions. Subtracting Eq. (13) from Eq. (26) yields

$$\hat{D}((\theta - \tilde{\theta}) \otimes I_m)h_{(m)}(t) = r_d(t) - r_f(t) - r_D(t) - r_u(t)$$

Based on the orthogonality and completeness properties of the Haar basis, the norm of all the remainders in the right-hand side of the above equation approach zeros when $m \to \infty$. This leads to,

$$\hat{D}((\theta - \tilde{\theta}) \otimes I_m) \to 0, \quad \textbf{as} \quad m \to \infty,$$

or

$$\Gamma_m(\theta - \tilde{\theta}) \to 0 \quad (27)$$

where $\Gamma_m \in R^{nm \times p}$. It is worthy to note that Γ_m has the same content as that of Eq. (15), except that here the matrix dimension is closes to infinity. From Eq. (27) one can conclude that provided that Γ_m is of full rank, $(\theta - \tilde{\theta}) \to 0$, and $\tilde{\theta} \to \theta$. It is evident that eventually Γ_m will be of full rank because in general nm is much larger than p. Hence, when the response and input signal carry sufficiently rich information, a full-rank Γ_m can be easily obtained, which in turn guarantees the convergence of the infinite Haar-based algorithms.

In practice, infinite dimensional representation of a function is not making much sense because it is difficult to implement numerically. Hence, the approximation approach, which applies finite dimensional space, is often adopted. This is what has been done in the off-line and on-line schemes presented here. The trade-off of the finite Haar expansion is that the identification is no longer as accurate as in the infinite-series case. Fortunately, when the signal is noise-free, *Bessel's inequality* [25] shows that every states or state functions in the state equations can be approximated by finite Haar series to some reasonable accuracy so far as *m* is large enough. As a consequence, the identification error induced from the truncated Haar series will depend on the number of the basis used. For the noise-free situations, better estimation accuracy can be obtained when the number of Haar basis is increased [22].

The identification accuracy will inevitably deteriorate when noise measurements are met in the real situations. Two types of noise are commonly seen in the experimental works. These are the random and interference type of noise. The former one belongs to high frequency regime while the latter one is often in low-frequency range. Our other study [26] indicated that the proposed algorithm is robust when the interference type of noise is facing. On the contrary, the identification error deteriorated when the random-type of noise was met. However, the experiments performed later in this study showed that by low-pass-filtering the raw data, the identification accuracy could be improved and the estimation convergence could be assured. The results are consistent with what have been observed in [22]. The approach also makes sense because so long as the bandwidth of the signals are limited, one can always find enough number of Haar basis to represent the signals to reasonable accuracy. Accurate estimates can be obtained accordingly. In the next section, numerical investigations focus on a simple numerical example is illustrated which is followed by experimental validations.

V. NUMERICAL VALIDATIONS

The system investigated here is the double-well potential problem that can be described quite adequately by a nonlinear differential equation of the Duffing type [27]:

$$\ddot{x} + \delta\dot{x} - \alpha x + \beta x^3 = A_o \omega^2 \cos(\omega t)$$

where α and β represent the linear and nonlinear components of the system stiffness while δ indicates the viscous damping effect. These coefficients are assumed to be the un-identified parameters during the numerical study. Details of the system's behaviors and their associated analysis can be found in [27]. The equation shown above can be recast into the following state-vector form, which is ready for the identification process

$$\begin{bmatrix} \dot{x}_1 \\ \dot{x}_2 \end{bmatrix} = \begin{bmatrix} x_2 \\ 0 \end{bmatrix} + \begin{bmatrix} 0 & 0 & 0 \\ x_1 & -x_2 & -x_1^3 \end{bmatrix} \begin{bmatrix} \alpha \\ \delta \\ \beta \end{bmatrix} + \begin{bmatrix} 0 \\ 1 \end{bmatrix} A_0 \omega^2 \cos \omega t$$

Proper parameter values are applied to the MATLAB ODE solver to generate responses. During the numerical test, the following parameters were first adopted: $\alpha = 1896$, $\delta = 3.11$, $\beta = 7.41$, $\omega = 2\pi(10)$, and $A_0 = 3.0$. Then, in order to check whether the proposed algorithm can capture parameter variations, the above parameter values were switched to the following set of values: $\alpha = 2500$, $\delta = 4.72$, $\beta = 9.21$, $\omega = 2\pi(10)$, and $A_0 = 3.0$, in the same simulation trial. Both the state response and the input data were recorded in one batch. These data were then fed, in smaller batches, to the "on-line" identification algorithm. Thus, the numerical validations were performed in an off-line manner, although it was the on-line algorithm that was supposed to be scrutinized. The identification results are presented in Figs. 1-3.

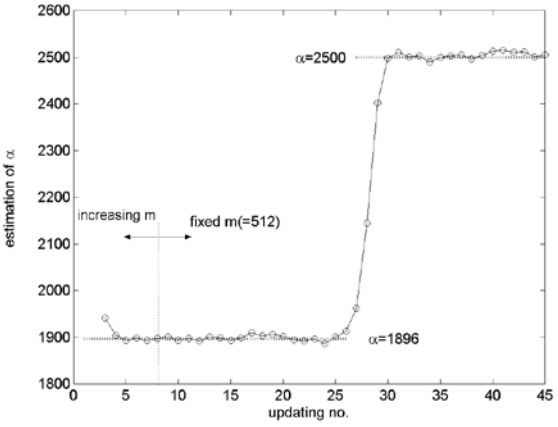

Fig. 1 The estimation of α of the numerical system

As mentioned previously, the proper number of Haar basis needed to expand a particular signal in fact depends on the characteristics of the signal and the accuracy required in the expansion. In order to gain an idea about what a proper *m* would be required in this example, m had been increased gradually in the power of 2 (also commencing from 2) during the identification process. The increment action terminated when the estimations seemed to converge. After that, *m* remained at that constant value throughout the rest of the process. As one can observe from Figures 1-3, the proper value of *m* is about 512, since the estimates essentially converge to the given value after *m* reached 512. After *m* was set to 512 and remained at that value, the iteration began, so did the data windowing action. Here, the window size *N* was equal to *m* (equal to 512). Therefore, the data-replacing ratio equated to one. The "unity-data-replacing ratio" means that at each updating step, an "old-data" vector of a length 256 will be given away while a "new-data" vector of the same length is joining in.

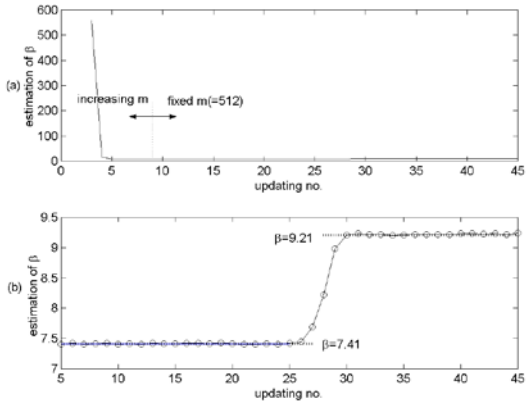

Fig. 2 The estimation of β of the numerical system

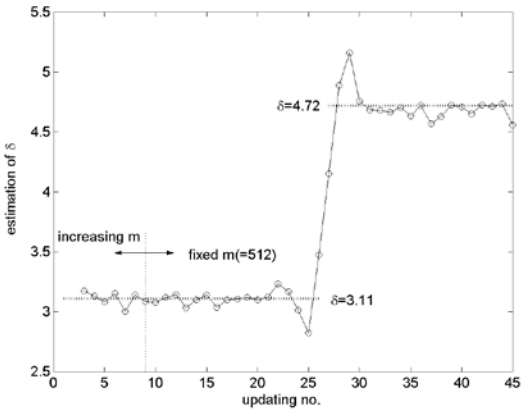

Fig. 3 The estimation of δ of the numerical system

From Figures 1-3, one can observe that the proposed algorithm not only accurately estimates the unknown parameter values but also captures the parameter variations. The parameter variations manifest themselves as abrupt jumps appearing in Figs. 1-3. The convergences of the estimates were fast. This is true no matter which parameter or what portions of the identification process are considered. Although all the estimates seem to fluctuate a little bit, they remain very close to the given values. It turns out that the largest errors of α and β are well below 1% while the largest error of δ is around 3.5%. These accuracies are quite acceptable.

It is worth to note that in Figs. 1-3, the "overall computing time" required in each updating was less than one second when *m* was taken as 512. Such a high

computation speed shows the feasibility of the proposed on-line identification algorithms. Next, the proposed schemes are further examined using an experimental system. Details of experimental study will be elaborated in the next section. In addition, although according to [21], rich initial conditions or persistent excitation conditions are required to guarantee a full rank Γ, and consequently the successful estimations. Our experiences show that it is in fact not difficult to gain successful estimations. The experiences are consistent with those reported in [21].

VI. EXPERIMENTAL VALIDATIONS

The experimental system is a mass-spring-damper system forced by a harmonic base motion. The base motion was generated by an electromagnetic exciter. Figure 4 shows a photograph of the experimental set-up. An important feature of the testing apparatus is that a U-shaped air curtain surrounds and supports the sliding mass of the system. There is no physical damper mounted in the system. Thus, the damping effect of the system which includes the viscous and dry-friction elements stems from the air resistance. The system can be modeled as the following

$$\tilde{m}\ddot{x} + c(t)\dot{x} + kx + F(t)\,\mathrm{sgn}(\dot{x}) = ku(t)$$

where $x(t)$, $\dot{x}(t)$, and $\ddot{x}(t)$ represent the dynamics associated with the sliding mass while $u(t)$ indicates the input base motion. $\tilde{m}$ denotes the system's inertia, and $c(t)$ and $F(t)$ designate the viscous-damping coefficient and the dry-friction force. The above differential equation can be recast into the following process-ready form

$$\begin{bmatrix}\dot{x}_1\\ \dot{x}_2\end{bmatrix} = \begin{bmatrix}x_2\\ 0\end{bmatrix} + \begin{bmatrix}0 & 0 & 0\\ -x_2 & -x_1 & -\tanh(\eta x_2)\end{bmatrix}\begin{bmatrix}-c(t)/\tilde{m}\\ -k/\tilde{m}\\ -F(t)/\tilde{m}\end{bmatrix} + \begin{bmatrix}0\\ 1/\tilde{m}\end{bmatrix}ku(t) \quad (28)$$

Here, the hyperbolic tangent function, $\tanh(\eta x_2)$, is used to replace the sign function. The former could be extremely close to the latter if η is large. In this study, η was taken as large as 55,000.

In order to examine whether the proposed algorithm can real-time capture parameter variations, we artificially disturbed parameter values during the experiments. The disturbances were produced by suddenly adding an extra mass on the top of the sliding mass. Therefore, $\tilde{m}$ has two constant values during the test. One was equal to the original sliding mass, 1.04 kg, while the other was equal to the sum of the two, namely 1.541 kg. Actually, $\tilde{m}$ is not the only parameter affected by the added mass. Since the sliding mass was supported by an air curtain, the size of the bottom gap between the sliding mass and the U-shaped guide would decrease (or increase) when the extra mass was put on (or removed from) the top of the sliding mass. These disturbances would presumably affect the viscous damping of the system. To that end, three parameter values were monitored during the experiments. They are $k/\tilde{m}$, $c(t)/\tilde{m}$, and $F(t)/\tilde{m}$.

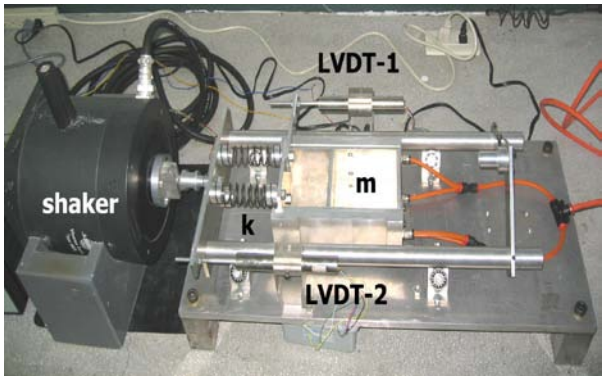

Fig. 4 The experimental system consists of helical springs, a sliding mass sitting on the top of a U-shaped guide, and a vibration shaker

Two LVDTs were mounted on the experimental system in order to measure the displacement responses of the sliding mass and the base excitation. In addition, to avoid the effects of high-frequency noise, a low-pass filter with the cut-off frequency equal to 100 Hz, was applied in the measuring process. The velocity response was obtained by differentiating the displacement response. The resultant velocity signal was then smoothened by a five-point moving average to reduce the fluctuations introduced by digital differentiation. Several MATLAB routines were coordinated with a LabVIEW program to carry out the identification calculations. Figures 5(a) and (b) show the input and output signals of the experimental system. The signals resemble a sinusoidal wave which can be verified in Figs. 5(c) and (d). From Figs. 5(a) and (b), one can observe that a disturbance occurred during 160 to 360 seconds which corresponded to the events of adding and removing the extra mass. One can also observe from Figs. 5(a) and (b) that when the shaker suddenly faced a greater inertia, its output decreased, so did the displacement of the sliding mass. The phenomenon makes sense if one considers that the eletromagnetic shaker itself is a mass-spring-damper system with finite stiffness. After the extra mass was removed, the amplitudes of the input and output responses simultaneously returned to their original levels.

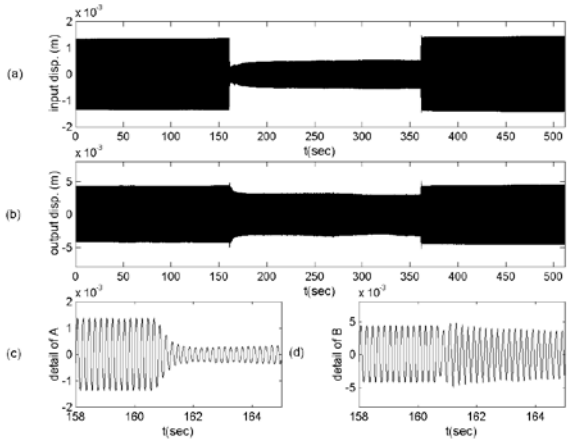

Fig. 5 The input and output signals that were fed to the on-line identification scheme

A process similar to the one used in the numerical study was adopted to determine the proper number of Haar basis

m and the window size N needed here. It turned out that m and N were both set to 512 while the data-replacing ratio was set to one. This means that the parameters were updated at every 256 sampling steps, which is approximately equivalent to 3 seconds because the sampling rate was 100 Hz. Although we never came across the limit of the proposed algorithms, the algorithms seemed to be comfortable in accomplishing the real-time identification tasks presented here. A rough estimation indicated that the computing speed of the proposed schemes was at least 30 times faster than the off-line ones when m was equal to 512. The experimental estimation results are presented in Figures 6-8.

Fig. 6 shows the real-time estimates of $k/\tilde{m}$, while Figures 7 and 8 present the counterparts of $c(t)/\tilde{m}$ and $F(t)/\tilde{m}$, separately. Noted that the value of k can be off-line estimated using the natural frequency of the system. The stiffness calculated from $\tilde{m}$ (1.04 kg) and the natural frequency of the system (5.97 Hz) was 1463 N/m. The estimates of k and $\tilde{m}$ are required in implementing the identification process which can be observed from Eq. (28). Based on the calculated k and the known $\tilde{m}$ (1.04 kg), the estimate of $k/\tilde{m}$ should be equal to $1463/1.04 \approx 1407$. Compared to this value, the result shown in Figure 6 was about 1330. The associated error was about 5.5 %, which is quite acceptable. On the other hand, when the extra mass was added, $\tilde{m}$ became 1.541 kg. As such, $k/\tilde{m}$ changed to $1463/1.541 \approx 950$. Figure 6 indicates that during this period, the identified $k/\tilde{m}$ value fluctuated slightly with a mean value close to 950. This again shows the reliability of the proposed algorithm. Moreover, Fig. 6 also demonstrates the fast convergences of the estimates when parameter variations occurred. Due to the presence of the air curtain, the viscous damping, $c(t)/\tilde{m}$ shown in Figure 7, was very low before the extra mass was added. Nonetheless, when the extra mass was added, the viscous damping suddenly increased to a higher level. The averaged value of $c(t)/\tilde{m}$ during that period was about 8.5. The increasing is reasonable since the size decrement occurred at the bottom gap of the air curtain

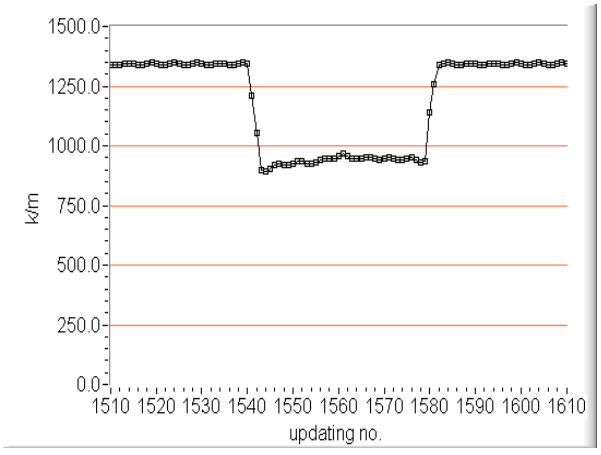

Fig. 6 The on-line $k/\tilde{m}$ identification of the experimental system

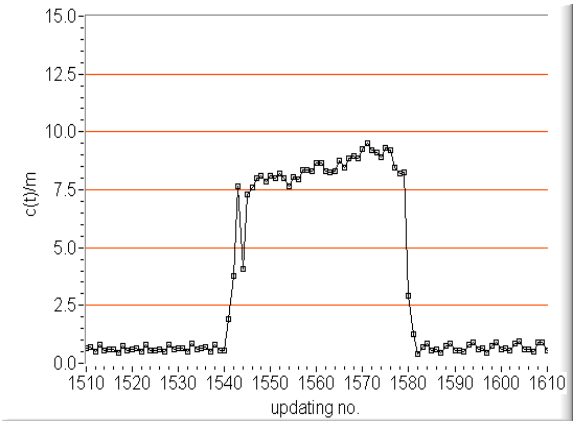

Fig. 7 The on-line $c(t)/\tilde{m}$ identification of the experimental system

Compared to $c(t)/\tilde{m}$, no obvious change except for two kinks had occurred on the estimates of $F(t)/\tilde{m}$, which is presented in Figure 8. The close-to-zero estimate of $F(t)/\tilde{m}$ makes sense, because the sliding mass was generally not in direct contact with the U-shaped guide. In contrast, the two kinks appearing at the beginning and ending of the disturbance could possibly be attributed to the temporary contacts between the sliding mass and the U-shaped guide. These contacts might be introduced by the lose motion of our hands in handling the extra mass.

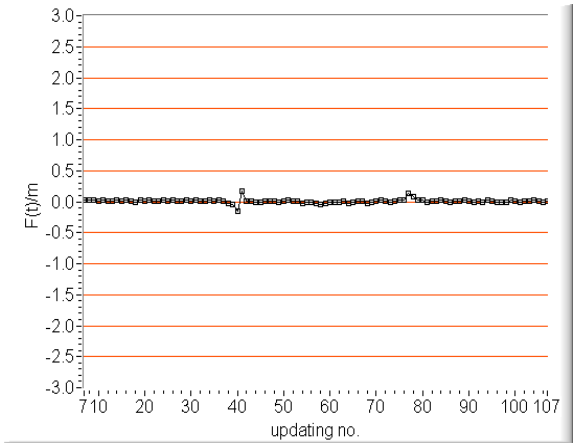

Fig. 8 The on-line $F(t)/\tilde{m}$ identification of the experimental system.

It is worth to note that because the velocity signal was obtained through digital differentiation, there were irregularities at the beginning and ending of each updating velocity vector. These irregularities caused the estimate to fluctuate with small amplitudes. The fluctuations can be seen as the ripple features appearing in Figures 6-8. Furthermore, although the computing speed seems to be quick enough for the experimental investigations, the speed can be improved further if better hardware and software were used.

VII. CONCLUSIONS

This paper proposes a new "on-line" identification algorithm which extends the existing off-line schemes developed in [21]. The values of the current study are two fold. Firstly, the computation efforts required in the off-line

schemes are greatly reduced by using the indirect matrix inversion schemes together with the recursive formula. Therefore, the on-line identification task can be tackled. The results indicate that roughly, the proposed algorithm is about 30 times faster than the original algorithm when m is taken as 512.

Secondly, the convergences of the off-line and on-line algorithms under the noise-free condition have been shown. For the infinite Haar series expansion, we show that the estimation can be perfect so long as Γ is of full rank. In contrast, when finite Haar expansion is adopted, we argue that the estimation errors are bounded although no specific forms of the bounds have been found. Regarding the noise issue, the proposed method is robust to the interference type of noise. When high-frequency random noise is facing, a low-pass filter can be applied to limit the bandwidth of the signal. Then, sufficient number of Haar basis can be collected to treat the problem in a regular way. The proposed algorithm is validated through numerical and experimental examples in which the results illustrate the reliability and effectiveness of the proposed schemes.

ACKNOWLEDGMENT

The author is indebted to Professor Shy-Leh Chen at National Chung Cheng University, Taiwan, Republic of China, for the valuable discussions of the off-line Haar-wavelet-based schemes and their possible applications on the on-line identifications. This research is supported by National Science Council, Taiwan, Republic of China, under grant number NSC-93-2212-E-131-001.

REFERENCES

S. M. Metev and V. P. Veiko, *Laser Assisted Microtechnology*, 2nd ed., R. M. Osgood, Jr., Ed. Berlin, Germany: Springer-Verlag, 2005.

S. Zhang, C. Zhu, J. K. O. Sin, and P. K. T. Mok, "A novel ultrathin elevated channel low-temperature poly-Si TFT," *IEEE Electron Device Lett.*, vol. 20, pp. 569–571, Nov. 2007.

O. Nelles, *Nonlinear System Identification*, Springer-Verlag, Berlin Heidelberg, 2001.

L. Ljung, *System Identification: Theory for the User*, Prentice-Hall, 1987.

S. Chen, S. A. Billings, W. Luo, "Orthogonal least squares methods and their application to non-linear system identification," *Int. J. Control*, vol. 50(5), pp. 1873-1896, 1989.

K. S. Mohammad, K. Worden, G. R. Tomlinson, "Direct parameter estimation for linear and non-linear structures," *Journal of Sound and Vibration*, vol. 152(3), pp. 471-499, 1992.

O. Gottlieb, M. Feldman, "Application of a Hilbert-transform based algorithm for parameter estimation of a nonlinear ocean system roll model," *Journal of Offshore Mechanics and Arctic Engineering*, vol.119, pp. 239-243, 1997.

M. Feldman, "Nonlinear free vibration identification via the Hilbert transformation," Journal of Sound and Vibration, vol. 208, pp. 475-489, 1997.

D. Remond, J. Neyrand, G. Aridon and R. Dufour, "On the improved use of Chebyshev expansion for mechanical system identification," *Mechanical System and Signal Processing*, vol. 22, pp. 390-407, 2008.

D. Alejo, L. Isidro, R. Jesús and A. Alvarez, "Parameter estimation of linear and nonlinear systems based on orthogonal series," *Procedia Engineering*, vol. 35, pp. 67-76, 2012.

R. P. Pacheco and V. Steffen Jr., "On the identification of non-linear mechanical systems using orthogonal functions," *Int. J. Non-linear Mechanics*, vol. 39, pp. 1147-1159, 2004.

C. Hwang, Y. P. Shih, "Laguerre operational matrices for fractional calculus and applications," *Int. J. Control*, vol. 34, pp. 557-584, 1981.

R. E. King, P. N. Paraskevopoulos, "Parameter identification of discrete time SISO systems," Int. J. Control, vol. 30, 1023-1029, 1979.

P. N. Paraskevopoulos, "Chebyshev series approach to system identification analysis and optimal control," *J. Franklin Inst.*, vol. 316, pp. 135-157, 1983.

P. N. Paraskevopoulos, P. D. Sparcis, S. G. Monroursos, "The Fourier series operational matrix of integration," *Int. J. System Sci*. vol.16, pp.171-176, 1985.

W. J. Staszewski, "Identification of non-linear systems using multi-scale ridges and skeletons of the wavelet transform," *Journal of Sound and Vibration*, vol. 214(4) pp. 639-658, 1998.

Y. Kitada, "Identification of non-linear structural dynamic systems using wavelets," *J. Engng Mech.*, vol. 124(10), pp. 1059-1066, 1998.

C. F. Chen, C. H. Hsiao, "Haar wavelet method for solving lumped and distributed parameter system," *IEE Proc.-Control Theory Appli*. Vol.144, pp.87-94, 1997.

C. F. Chen, C. H. Hsiao, "Wavelet approach to optimizing dynamic system," *IEE Proc.-Control Theory Appli*. Vol. 146, pp. 213-219, 1999.

C. H. Hsiao, W. J. Wang, "Haar wavelet approach to nonlinear stiff systems," *Mathematics and Computers in Simulation*, vol. 57, pp. 347-353, 2001.

C. H. Hsiao, W. J. Wang, "State analysis of time-varying singular bilinear systems via Haar wavelets," *Mathematics and Computers in Simulation*, vol.52, pp. 11-20, 2000.

C. H. Hsiao, "State analysis of linear time delayed systems via Haar wavelets," *Mathematics and Computers in Simulation*, vol.44, pp. 457-470, 1997.

S. L. Chen, J. W. Liang and K. C. Ho, "Parameter identification of nonlinear systems by Haar wavelet: Theory and Experimental Validation," *ASME Journal of Vibration and Acoustics*, vol. 134, pp. 031005-1-031005-12, 2012.

S. L. Chen, H. C. Lai, K. C. Ho, "Identification of linear time varying systems by Haar wavelets," *International Journal of Systems Science*, vol. 37, pp.619-628, 2006.

W. T. Wu, L. Y. Juang, "On recursive parameter estimation of multivariable systems," *J. Chin. Inst. Eng*. Vol.3, pp. 89-93, 1980.

J. H. Chou, J. H. Sun, J. N. Shieh, On-line identification and optimal control of continuous-time systems, *Mathematics and Computers in Simulation*, vol. 63, pp. 493-503, 2003.

M. Pedersen, *Functional analysis in applied mathematics and engineering*, Chapman & Hall/CRC, 2000.

J. W. Liang, "Identifying damping from multiple degree-of-freedom vibrations system via energy-balance and Haar-based-expansion methods," *Proceedings of The 29th National Conference on Theoretical and Applied*

Mechanics, TAIWAN, Dec. 2005.

F. C. Moon, *Chaotic Vibrations: An Introduction for Applied Scientist and Engineers*, John Wiley and Sons, New York, 1987.

M. Wegmuller, J. P. von der Weid, P. Oberson, and N. Gisin, "High resolution fiber distributed measurements with coherent OFDR," in *Proc. ECOC'00*, paper 11.3.4, pp. 109, 2000.

Jin-Wei Liang received his PhD degree in Mechanical Engineering from Michigan State University, East Lansing, in 1996. He has been with Ming Chi University of Technology since 1985 in which he is currently a Professor in the Department of Mechanical Engineering and Dean of College of Engineering. His research interests include intelligent control, nonlinear dynamics and control, damping estimation in vibration systems.